*Polymers for Advanced Technologies*

WILEY

polymers advanced technologies

RESEARCH ARTICLE

# Enhancement of Mechanical and Thermo-Physical Properties in CNTs/GO-Coated Carbon Fiber-Reinforced Epoxy Composites

Mayank Singh[1,2] | Srihari Dodla[2] | R. K. Gautam[2] | Pushkar Jha[3]

[1]Department of Mechanical Engineering, Dr. D.Y. Patil Institute of Technology, Pune, India | [2]Department of Mechanical Engineering, Indian Institute of Technology (BHU), Varanasi, India | [3]School of Mechanical Engineering, KIIT Deemed to be University, Bhubaneswar, India

**Correspondence:** Srihari Dodla (sdodla.mec@iitbhu.ac.in)

**Received:** 28 October 2024 | **Revised:** 18 June 2025 | **Accepted:** 4 August 2025

**Funding:** This work was supported by Science and Engineering Research Board (SRG/2020/001811) and Defence Research and Development Organisation (DFTM/10/3855/M/12/PM-10/003/D (R&D)).

**Keywords:** carbon fibers | carbon nanotubes | graphene oxide | mechanical testing | tribological behavior

## ABSTRACT

This study predominantly focuses on the application of carbon nanotubes (CNTs), graphene oxide (GO), and hybrid (CNTs/GO) onto carbon fibers through a spray coating process and examines the resulting impact of the coating on mechanical, tribological, and thermo-physical properties of polymer composite. The synergetic effect of two-dimensional GO and one-dimensional CNTs forms a three-dimensional network structure, resulting in significant enhancements in the mechanical and interfacial properties of fiber-reinforced polymer composites. The CNTs/GO hybrid coated carbon fiber reinforced epoxy (HCFRE) composite demonstrates superior performance in interlaminar shear strength (ILSS), flexural strength, tensile strength, and hardness, with an enhancement of 38.73%, 30.40%, 33.53%, and 32.64%, respectively, compared to carbon fiber reinforced epoxy (CFRE) composite. The fracture toughness, tensile, and flexural modulus of the HCFRE composite have improvements of 36.36%, 31.66%, and 57.68%, respectively, as compared to the CFRE composite. The HCFRE obtained the maximum thermal conductivity with a 44.44% increment compared to the CFRE composite. The tribological tests comprise four distinct sliding frequencies (6, 8, 10, and 12 Hz) and normal loads (30, 40, 50, and 60 N) with a consistent stroke length of 1.5 mm. Worn-out surfaces are studied by scanning electron microscope (SEM) images. For the HCFRE, the specific wear rate was decreased by 42.84% compared to the CFRE composite. As the normal load increases, the friction coefficient also increases, whereas it decreases with sliding frequencies.

## 1 | Introduction

Polymer and polymer composite materials (PCMs) have gained growing favor in various structural and engineering domains, such as the automotive and aerospace industries, as well as in agriculture. The primary reasons for this preference are their excellent combination of strength-to-weight ratio, stiffness, versatility, and cost-efficiency [1]. Previous studies have extensively investigated various types of fabric-based polymer composites, including aramid fabric (AF), glass fabric (GF), hybrid fabrics, carbon fiber (CF), and polyester fabric [2–5]. Carbon fiber (CF) stands out as a promising choice among these fabrics for reinforcement due to its impressive attributes, such as excellent thermal conductivity, high modulus, and high strength, all of which offer advantages for improving tribological properties [6, 7]. Moreover, some researchers have also noted the lubricious nature of carbon fiber [6, 8]. Polymer composites incorporating carbon fiber reinforcements can be crafted using various configurations like unidirectional, biaxial, chopped, and woven mats. These are combined with

thermoset matrices such as phenolic, polyester, or epoxy [9]. Epoxy resins, in particular, are the most commonly employed matrix system for producing polymer composites in various engineering applications. This popularity stems from their strong adhesion, excellent dimensional stability, and outstanding resistance to both chemical and thermal factors. It is widely recognized that, besides the inherent qualities of the reinforcement and the matrix, the overall performance of composite materials is significantly influenced by the bond quality at their interface. A robust interfacial bond is vital for efficient load transfer from the matrix to the fibers, preventing stress concentration and bolstering overall mechanical performance [10, 11]. Moreover, the interfacial properties of the fiber-matrix combination significantly influence impact strength, compressive strength, failure strain, fatigue resistance, fracture toughness, and damage initiation threshold [12, 13]. However, carbon fiber (CF) typically exhibits low surface energy and inadequate wettability due to its non-polar, chemically inert structure with highly crystallized graphitic basal planes. As a result, it often experiences weak interactions with most polymers [14]. In fiber-reinforced polymer composites, higher mechanical strength generally correlates with improved wear resistance, crucial for durability-focused applications. Strong fiber-matrix bonding enhances cohesion, reducing surface degradation under friction. High-strength composites also withstand greater loads with minimal deformation, maintaining surface integrity and minimizing wear-induced damage like cracks or delamination. Additionally, they dissipate energy more effectively during frictional interactions, decreasing material removal. However, factors such as fiber type, matrix composition, and environmental conditions also significantly influence wear performance [15, 16].

Various techniques have been employed to enhance the adhesion of CF within the polymer matrix. In the last few years, significant attention has been directed toward incorporating nanoparticles into carbon fiber (CF) reinforcement composites. This heightened interest is primarily driven by nanoparticles' remarkable mechanical properties and reinforcement capabilities. Simulation studies have also revealed that integrating nanoparticles into CF composites can mitigate stress concentrations at the interfaces, leading to improvements in their mechanical and tribological characteristics [17]. Previous research has specifically highlighted the positive effects of introducing graphene nanoplates (GNPs) [18] and carbon nanotubes (CNTs) [19] into the sizing process, demonstrating enhancements in both the mechanical and interfacial attributes of polymer composites reinforced with carbon fibers (CFRP). CNTs in their one-dimensional (1D) form exhibit notable characteristics such as a large surface area, flexibility, and exceptional strength. Given these attributes, CNTs show great potential in improving interface characteristics and creating versatile composite reinforcements with carbon fibers. This is attributed to the outstanding mechanical, electrical, and thermal properties inherent in CNTs [20–22]. Numerous research studies have indicated that incorporating CNTs into sizing solutions significantly improves carbon fiber-reinforced composites' interfacial and mechanical properties. This enhancement is credited to the increased chemical bonding and mechanical interlocking established between carbon fibers and the matrix [23]. In the research conducted by Li et al. [24] CNTs were utilized to coat the surface of carbon fibers using an aqueous suspension deposition process. In this approach, CNTs served to address surface irregularities on the carbon fibers and acted as connectors between the fibers and the matrix, thereby diminishing stress concentrations. GNPs, which consist of a single layer of carbon atoms arranged in a two-dimensional lattice structure, have garnered considerable interest in recent times owing to their impressive specific surface area, exceptional mechanical characteristics, and conductivity [25]. Researchers have increasingly employed 2D GNPs for the modification of carbon fibers (CF) and CF/epoxy composites. For instance, the incorporation of GO sheets into the fiber sizing solution has significantly bolstered the interfacial adhesion between carbon fibers and the polymer matrix, thereby enhancing their mechanical properties [26]. Furthermore, integrating GNPs at the fiber-matrix interface yields significant effects on the mechanical and thermal properties of the composite [27]. The stacking and aggregation of distinct graphene layers in GNPs are primarily driven by van der Waals interactions. Graphene oxide sheets can impede initial crack formation, reducing stress intensity factors at the crack tips [28]. Studies have confirmed that the addition of GNPs and CNTs as reinforcement materials can improve the frictional characteristics and wear resistance by improving mechanical interlocking between the matrix and fiber [29, 30]. The literature mentioned previously highlights that enhancing the composite's performance is achievable by incorporating micro and nanofillers. The prevailing approach in the majority of studies involves directly incorporating nanoparticles into the epoxy for the purpose of polymer modification. These investigations consistently demonstrate that adding these nanofillers improves the polymer composites' mechanical, tribological, and thermal performance. To the best of our knowledge, there is limited existing research on the fabrication of composites reinforced with coated nanoparticles and hybrid nanoparticles on fiber to improve the mechanical interlocking and interfacial adhesion between the matrix and fiber. Among these studies, a noteworthy observation is that while hybrid nanoparticles have been commonly employed to modify epoxy, particularly as discussed earlier, there has been relatively less exploration into utilizing hybrid coatings of nanoparticles on carbon fiber (CF) surfaces.

## 2 | Experimental Approaches

### 2.1 | Materials

In this research, epoxy resin LY 556 (with a density of 1.1 g/cm$^3$) and hardener HY 917 were utilized, sourced from Ciba Gaigy Limited in Mumbai, India. A carbon fiber mat weighing 200 Gsm, featuring a bi-directional plain pattern, was obtained from Arrow Technical Textiles, Mumbai, India. As per the supplier's specifications, the fiber possesses a density of 1.8 g/cm$^3$ and an individual fiber diameter measuring 8 μm. CNTs nanoparticles were sourced from TUHH in Hamburg, Germany, with an average inner diameter of ±6.5 nm, an outer average diameter of ±40 nm, and an approximate length of ±2 μm. These nanoparticles underwent functionalization through a chemical treatment method, and the specifics of the functionalization process are elaborated in section [31]. Research grade graphene oxide (GO) nanoparticles (purity: +99%, thickness 0.8–2 nm, and length 5–10 μm) were provided from shilpent. SEM images of both CNTs and GO are shown in Figure 1. Acetone, obtained

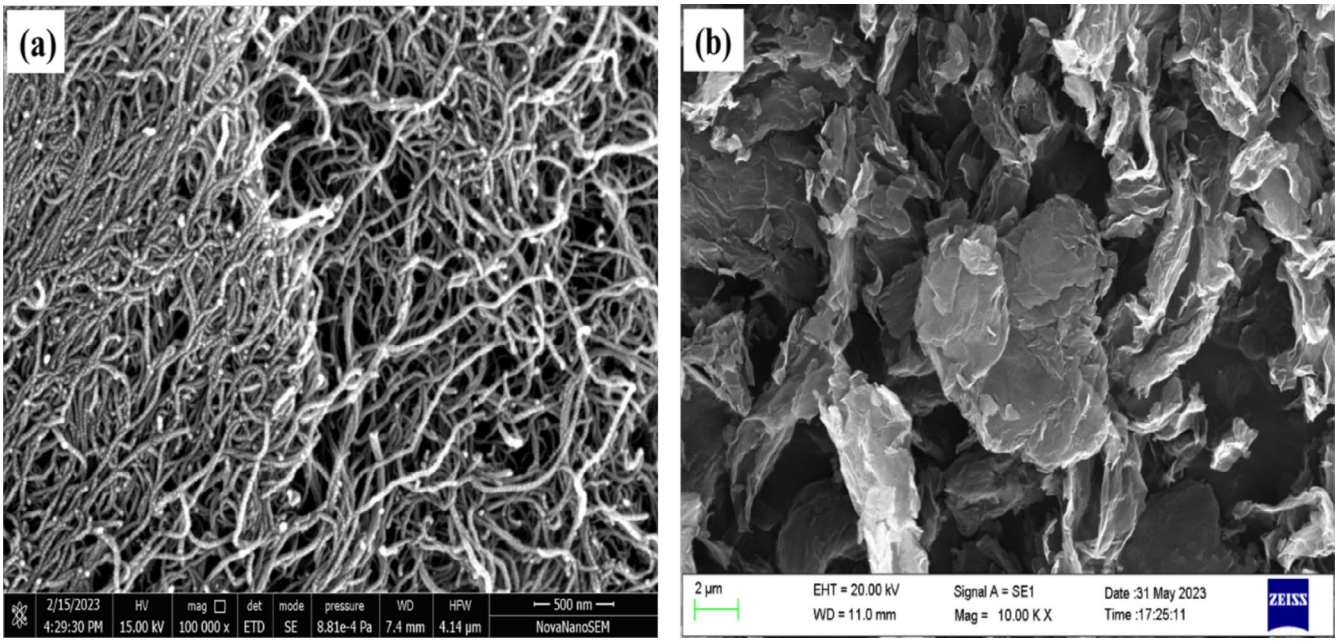


**FIGURE 1** | SEM image of (a) CNTs and (b) GO.

from Sigma Aldrich, was employed as a solvent and cleansing agent in the experiment.

## 2.2 | Surface Modification of Carbon Fiber by the Spray Coating of CNTs, GO, and CNTs/GO Hybrid Nanoparticles

Before the spray coating process, the carbon fiber was treated with acetone to remove the sizing agents. Then, it was repeatedly washed in deionized water and dried at ambient temperature to obtain the desized CF. After that, the three distinct solutions were prepared by mixing 1 mg/mL of CNTs in acetone, 1 mg/mL of GO in acetone, and a combination of 1 mg/mL of CNTs/GO hybrid (in ratio 1:1) in acetone. The stirring process, facilitated by a magnetic stirrer, lasted for 10 min to ensure uniform dispersion of nanoparticles in the solvent. Subsequently, the mixture underwent a 1-h bath sonication process, utilizing high-sound wave frequency to disperse any agglomerates and achieve proper dispersion of nanoparticles in acetone. A well-dispersed nanoparticle-acetone solution was sprayed onto 20 × 20 mm carbon fiber samples using a high-atomizing spray cannon connected to an air compressor. During the coating process, a 0.5 mm diameter nozzle was maintained perpendicular to the fiber surface at a fixed distance of 12 cm to ensure consistent particle impact energy, minimize overspray, and avoid fluctuations in droplet size and dispersion. The system operated at a constant air pressure of 3.0 bar to ensure stable atomization. The nanoparticle suspension was applied at a controlled flow rate of 0.2 mL/s for 2 min on each side, enabling uniform and homogeneous coating across the fiber surface. After the spray coating, the solvent was removed through drying, leading to the immobilization of nanoparticles on the carbon fiber surface. The spray coating process was shown in Figure 2. Three different types of coatings were applied to the carbon fiber: (1) a 1 wt% concentration of CNTs, (2) a 1 wt% concentration of GO, and (3) a 1 wt% concentration of CNTs/GO hybrid (in ratio 1:1).

## 2.3 | Fabrication of Fiber-Reinforced Polymer Composites

Four distinct polymer composite samples were created: Carbon Fiber Reinforced Epoxy (CFRE), Carbon Nanotubes Coated Carbon Fiber Reinforced Epoxy (CCFRE), Graphene Oxide Coated Carbon Fiber Reinforced Epoxy (GCFRE), and Hybrid (CNTs/GO) Coated Carbon Fiber Reinforced Epoxy (HCFRE). Each sample consisted of six layers. The fabrication process involved preparing a precisely calculated blend mixture of epoxy and hardener in a beaker, maintaining a weight ratio of 10:1. This ensured the initiation of the appropriate chemical reaction when applied to the fiber mat. The hand lay-up method, as shown in Figure 2, was employed in the fabrication process of the polymer composites. During this process, epoxy resin was systematically applied to each layer sequence for all samples. A pressure of 15 KPa was applied to the samples on the upper face in order to stop the epoxy resin from depositing and make sure there were no dry fiber patches. Subsequently, the samples underwent compression for 24 h during the curing phase, followed by an additional 30 h of curing in a naturalistic environment. This meticulous process aimed to produce polymer composite materials with specific properties tailored to each type of coating.

## 2.4 | Characterization

### 2.4.1 | Thermogravimetric Analysis (TGA)

The thermal stability of both the CF and the CF coated with nanoparticles was analyzed using a TGA-50 instrument provided by Shimadzu Asia Pacific Pvt. Ltd. Samples weighing between 1.143 and 1.955 mg were heated at a rate of 10°C per minute, within a temperature range of 24°C–800°C, to create TGA curves. Nitrogen gas was used to keep the atmosphere inert throughout this procedure. This analytical method made it easier to examine the behavior of the sample at different heat conditions.

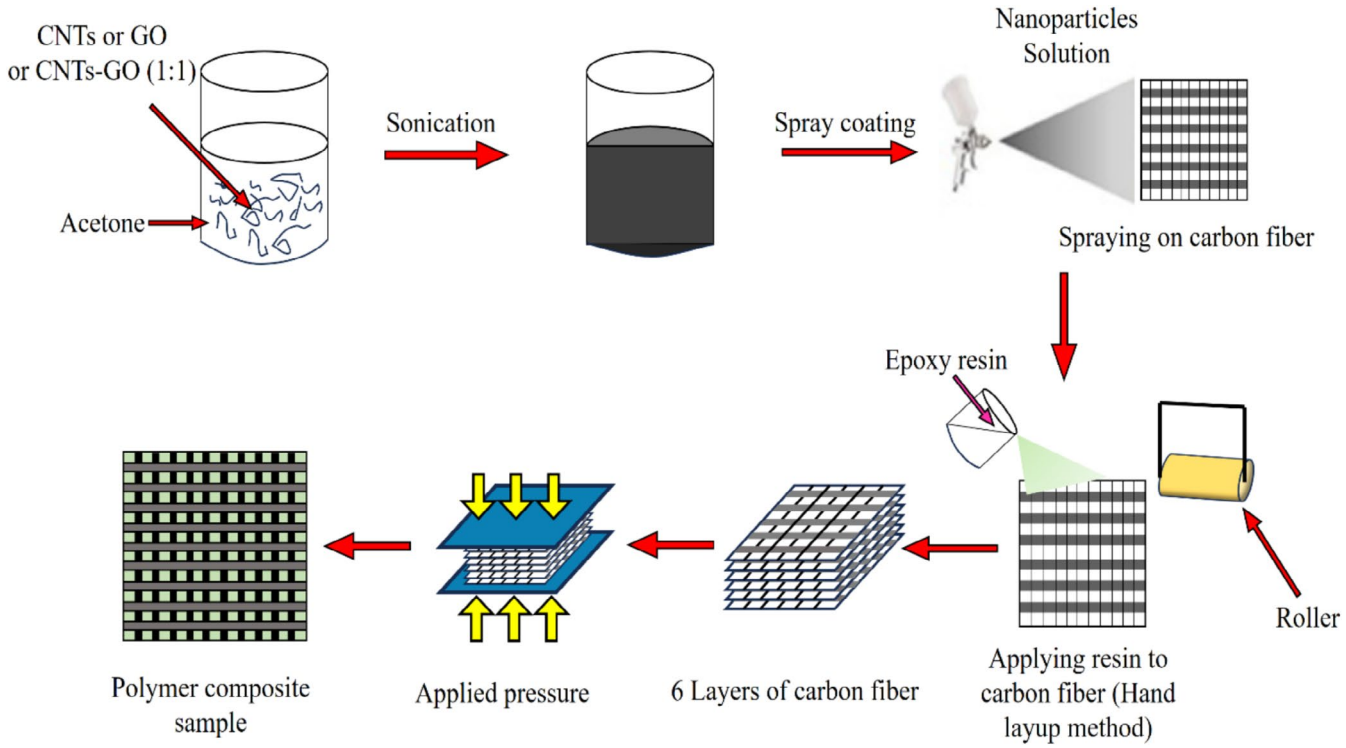


**FIGURE 2** | Schematic diagram for surface modification of fiber and fabrication of polymer composites.

#### 2.4.2 | Scanning Electron Microscopy (SEM)

SEM analysis was conducted to investigate the morphological features of both uncoated and nanoparticle-coated carbon fiber. Additionally, a thorough examination of the wear surface of specimens from polymer composites was carried out using scanning electron microscope images. A 20 kV EVO-SEM MA15/18 from Carl Zeiss Microscopy Ltd. was used for the evaluation.

#### 2.4.3 | Density Calculation

Following the ASTM D792-13 standard was followed in order to calculate the sample density. The mass of the sample of (20*20*2) mm in dimensions was measured using a digital weighing machine that had an accuracy of 0.1 mg. The density was then determined by applying Archimedes' principles and the sample mass. This process yielded standard values for both the sample mass and the calculated density.

#### 2.4.4 | Vickers Microhardness Testing

A micro-hardness tester was used to find the hardness of four distinct polymer composite samples of (20*20*2) mm in dimensions. Applying a 25 g load and dwell time of 10 s produced the indentations. Every sample of the polymer composite underwent 10 separate microhardness tests, with the average result being noted.

#### 2.4.5 | Tensile Testing

A computer-controlled Instron universal testing equipment with a 100 kN load cell was used to perform tensile tests on the composite specimens. The testing followed the guidelines as per ASTM D-3039 standard, employing test specimens measuring (150*15*2) mm in dimensions. The testing process was conducted with a cross-head speed of 2 mm/min and at room temperature.

#### 2.4.6 | Flexural Testing

Following the ASTM D-790 standard, the flexural tests of the composite specimens were performed using a computer-controlled Instron universal testing machine. The composite specimens of (120*15*2) mm in dimensions; flexural characteristics were evaluated at a span length of 60 mm and a cross-head speed of 2 mm/min.

#### 2.4.7 | Short Beam Shear Test

The composite specimens' Interlaminar Shear Strength (ILSS), with dimensions of 15 mm in width and 30 mm in length, was assessed through short-beam shear testing conducted on an Instron universal testing machine. The cross-head speed was adjusted to 1 mm/min during the testing process; this adhered to the parameters specified in the ASTM D-2344 standard.

#### 2.4.8 | Izod Impact Test

Izod impact testing used a Resil Impactor-50 model from CEAST, S.p.A., Italy. The test parameters included an impact length of 0.327 m and a velocity of 3.426 $ms^{-1}$. A hammer with a mass of 0.932 kg was dropped onto the specimens of (64*12.7*2) mm in dimensions, and impact strength was determined according to ASTM D256 standards. The specimens were positioned in the

testing machine so that the notch root aligned with the vice, and the hammer impacted the notched face.

#### 2.4.9 | Thermal Conductivity Test

The polymer composites' thermal conductivity (k), arranged in a stacked configuration, was measured using a TPS 500 thermal conductivity analyzer of (20*20) mm sample size. This instrument provided a direct assessment of the thermal conductivity (k) value at ambient room temperature.

#### 2.4.10 | Tribological Testing

Wear tests using linear reciprocating motion were conducted in accordance with ASTM G133 guidelines. A square sample, 20 mm by 20 mm in size and 2 mm thick, was used for the testing. Polymer composite specimens that were fixed were subjected to the reciprocating friction test. The counter surface material was a 62 HRC chrome steel ball that reciprocated on the stationary sample. The experiments utilized a reciprocating friction monitor (TE 200ST) sourced from Magnum Engineers, Bangalore, India. The stroke length stayed at 1.5 mm throughout the testing period. Various tests were conducted under different parameters, encompassing four distinct frequencies (6, 8, 10, and 12 Hz) and four distinct loads (30, 40, 50, and 60 N). The test period was 20 min for each test, during which the wear loss and coefficient of friction were carefully examined.

## 3 | Results and Discussion

### 3.1 | Thermogravimetric Analysis of Carbon Fiber and Nanoparticles Coated Carbon Fiber

Figure 3 illustrates the TGA curves for both the carbon fiber and the carbon fiber coated with nanoparticles. In these curves, the plateau region indicates the thermal stability range of the fiber, while the steep section corresponds to the phase of weight loss. As seen in Figure 3, the thermogravimetric curves, which range in temperature from 24°C to 800°C, may be separated into two phases. The first stage of thermal degradation is linked to the extraction of moisture content and waxy components from the fibers, and it happens between 24°C and 550°C. Both uncoated and nanoparticle-coated carbon fiber lose about 1%–3% of its weight in this temperature range [32]. Carbon fiber remains stable up to 550°C in air, beyond which rapid decomposition occurs due to the oxidation of carbon fiber [33, 34]. In the temperature range of 550°C–800°C, uncoated carbon fiber undergoes an 11.2% weight loss, while CNTs-coated, GO-coated, and CNTs/GO-coated carbon fibers experience reduced weight losses of 8.21%, 7.21%, and 6.12%, respectively. The protective barriers provided by GO and CNTs contribute to enhanced thermal stability. The total weight losses for uncoated, CNTs-coated, GO-coated, and CNTs/GO-coated carbon fibers are 13%, 11.21%, 10.21%, and 8.45%, respectively. Incorporating CNTs and GO improves heat resistance, which is attributed to their exceptional thermal properties [35]. The enhanced thermal stability is associated with the facilitation of heat dissipation by CNTs and GO, preventing the formation of localized hot spots in coated carbon fiber [36, 37].

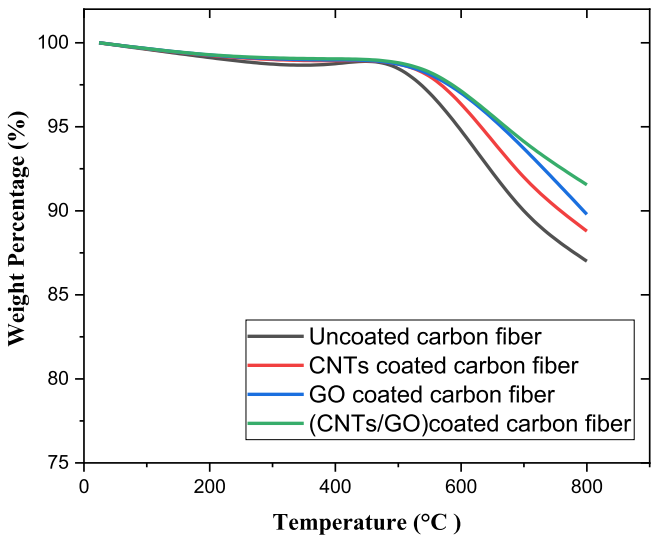


**FIGURE 3** | TGA curves of uncoated carbon fiber, CNT-coated aramid fiber, GO-coated carbon fiber, and (CNTs/GO) hybrid-coated carbon fiber.

### 3.2 | Scanning Electron Microscopy (SEM)

The surface morphologies of CF, GO-coated CF, CNTs-coated CF, and CNTs/GO hybrid-coated CF are shown in Figure 4. Because of the Polyacrylonitrile precursor spinning process, the surface of the non-coated CF (Figure 4a) has continuous ridges and grooves running down the fiber axis, giving the impression of being relatively smooth. The introduction of carbon nanomaterials alters the surface topography of CF. In (Figure 4b), CNTs exhibited a random orientation, wrapping around the surfaces of carbon fibers (CF) with minimal aggregation. This resulted in the formation of a rough surface characterized by numerous protrusions [38]. Under the same modification circumstances, GO is equally distributed over CF surfaces (Figure 4c). The CNTs/GO hybrid coating layer (Figure 4d) shows a uniform distribution on CF surfaces. The attachment of CNTs and GO to CF surfaces enhances surface contact points and interactions between CF and the epoxy matrix. This enhancement is beneficial for improving the mechanical and interfacial properties of carbon fiber-reinforced epoxy (CFRE) composites [39].

### 3.3 | Density Calculation

The four different polymer composites exhibited specific gravities and densities, as detailed in Table 1. The average density of CFRE, CCFRE, GCFRE, and HCFRE composite samples was determined to be 1323.1187, 1281.89275, 1312.5006, and 1300.088 kg/m$^3$, respectively. Compared to the other four polymer composites, CCFRE exhibits the lowest density, while CFRE displays the highest density.

### 3.4 | Microhardness Test

The sample's surface was marked with 10 different indentations, and measurements of the microhardness were made at each

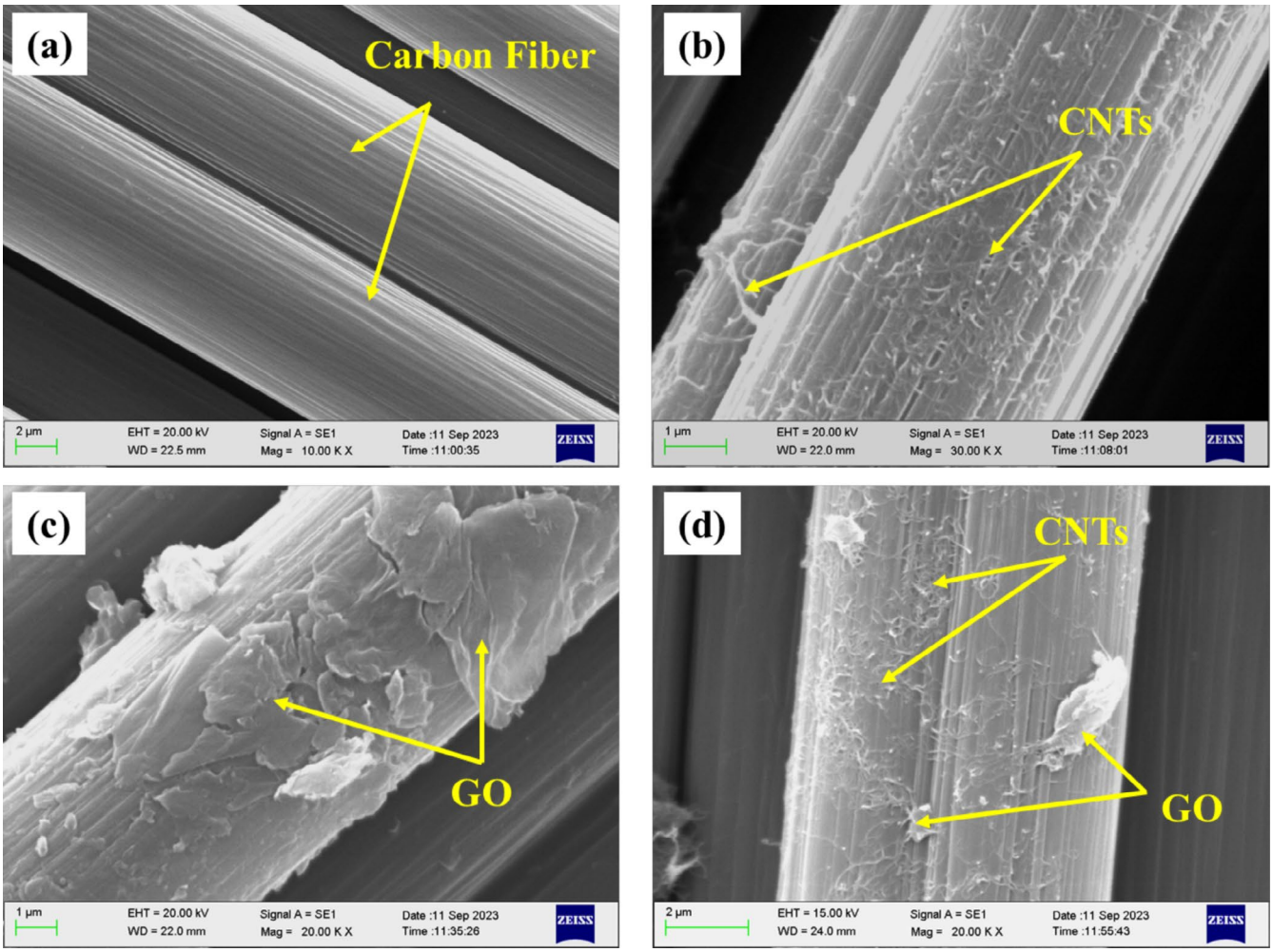


**FIGURE 4** | The surface morphology of carbon fiber (a) uncoated CF, (b) CNTs coated CF, (c) GO coated CF, (d) CNTs/GO hybrid coated CF.

location. The hardness of the specimens was then determined by averaging the 10 values. This data were presented on a bar chart in Figure 5, including the standard deviation for each measurement. Figure 5 compares hardness values among four types of polymer composites. CFRE exhibited the lowest hardness value, measured at 20.83 HV. The increase in hardness values observed in the polymer composites can be attributed to the coating of nanoparticles on the fibers. This coating enhances the interfacial bonding between the matrix and fibers, which reduces the mobility of interface shear bonds and helps mitigate deformation induced by external forces, consequently enhancing the hardness of the polymer composite [38]. The hardness of HCFRE surpassed all other polymer composites, showing a remarkable 32.64% increase compared to CFRE. This notable enhancement in hardness is attributed to the synergistic and bridging effects of 1-D (CNTs) and 2-D (GO) present in the composites [40].

### 3.5 | Tensile Testing

Five specimens were subjected to tensile testing for each type of polymer composite, including CFRE, CCFRE, GCFRE, and HCFRE, to assess the impact of woven carbon fiber and nanoparticles-coated carbon fibers on the resulting composite laminates' tensile properties. The stress–strain curves for these specimens are illustrated in Figure 6, indicating the brittleness of the composite as evidenced by the measured strain levels. Incorporating CNTs/GO increased the brittleness while enhancing the composite's strength, which is reflected in higher failure stress.

Figure 7a,b show the tensile strength and tensile modulus obtained from the stress–strain curve analysis, respectively. Notably, CCFRE, GCFRE, and HCFRE exhibit superior tensile strength and modulus compared to CFRE, indicating the reinforcing effect of CNTs/GO. CCFRE significantly enhances tensile modulus and tensile strength, surpassing CFRE by 25.95% and 27.94%, respectively. The kinked and twisted structure of CNTs, which creates mechanical interlocks with the matrix, is credited with this enhancement [41], preventing polymer chain movement under load and enhancing tensile properties [42]. Similarly, GCFRE displays increased tensile modulus and strength with improvements of 22.33% and 23.22%, respectively, relative to CFRE. The reason for this improvement is the layered and wrinkled sheet structure of GO, which prevents cracks from propagating inside the polymer matrix and increases energy dissipation [43]. Moreover, CCFRE exhibits higher tensile strength and modulus compared to GCFRE, primarily due to GO's tendency to aggregate owing to its larger surface area [44].

**TABLE 1** | Density calculation of CFRE, CCFRE, GCFRE, and HCFRE composites.

| S. no | CFRE (mass in air) (gm) | CFRE (mass immersed in liquid) (gm) | Specific gravity | Density (kg/m$^3$) |
|---|---|---|---|---|
| 1. | 1.706 | 0.422 | 1.3286 | 1324.6142 |
| 2. | 1.708 | 0.421 | 1.3256 | 1321.6232 |
| **S. no** | **CCFRE (mass in air) (gm)** | **CCFRE (mass immersed in liquid) (gm)** | **Specific gravity** | **Density (kg/m$^3$)** |
| 1. | 2.260 | 0.503 | 1.2862 | 1282.3414 |
| 2. | 2.257 | 0.501 | 1.2853 | 1281.4441 |
| **S. no** | **GCFRE (mass in air) (gm)** | **GCFRE (mass immersed in liquid) (gm)** | **Specific gravity** | **Density (kg/m$^3$)** |
| 1. | 1.729 | 0.417 | 1.3178 | 1313.8466 |
| 2. | 1.732 | 0.415 | 1.3151 | 1311.1547 |
| **S. no** | **HCFRE (mass in air) (gm)** | **HCFRE (mass immersed in liquid) (gm)** | **Specific gravity** | **Density (kg/m$^3$)** |
| 1. | 1.762 | 0.412 | 1.3051 | 1301.1847 |
| 2. | 1.759 | 0.409 | 1.3029 | 1298.9913 |

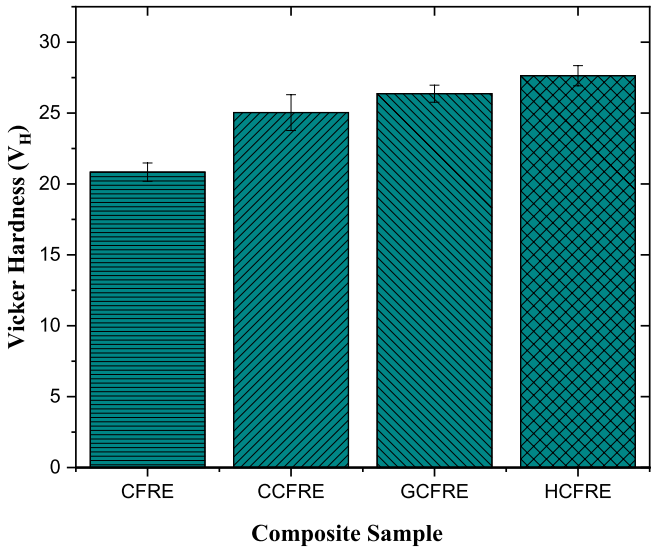


**FIGURE 5** | Vickers hardness value of different fiber reinforced polymer composites.

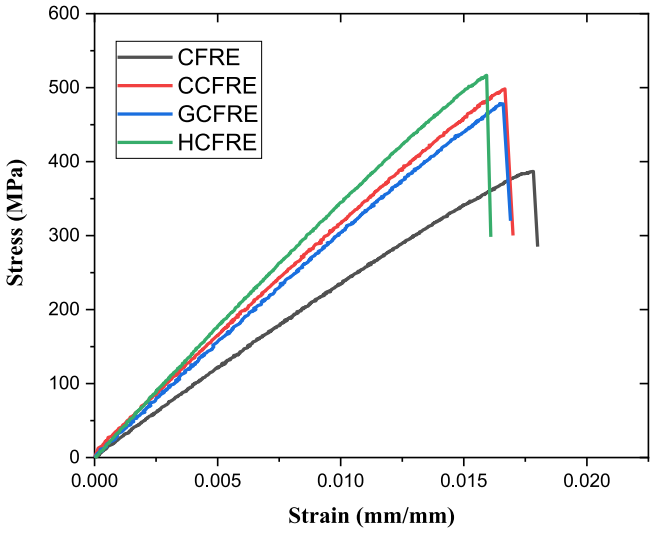


**FIGURE 6** | Stress–strain curves of different fiber-reinforced polymer composites.

According to Figures 6 and 7, HCFRE demonstrates the highest tensile modulus of 33.06 GPa and tensile strength of 518.09 MPa among all four composite specimens. This represents an increase of 33.53% tensile strength and 31.66% tensile modulus as compared to CFRE. Combining one-dimensional CNTs and two-dimensional GO structures facilitates the formation of a rod-sheet network, synergistically enhancing the composite's tensile properties [43]. The tensile strength of polymer composite laminates is bolstered by factors such as the durability of the matrix material, the level of interfacial adhesion, and the effective dispersion of particles or fibers within the matrix [45]. CF smooth surface usually shows poor interfacial adhesion between the fiber strand and matrix. Nevertheless, better interfacial bonding between the fiber and epoxy is produced by the deposition of CNTs or GO onto CF, allowing for more efficient stress transmission from the epoxy to the fiber [19]. The remarkable mechanical properties of CNTs and GO are also instrumental in enhancing the tensile properties of the epoxy composite [46].

### 3.6 | Flexural Testing

The flexural stiffness and strength play a critical role in ensuring the structural integrity of composites, particularly in scenarios involving high loads and sliding velocities, where preventing deformation and bending failure is paramount. To address this concern, the flexural characteristics of CFRE composites, both with and without coatings of CNTs, GO, and a hybrid of GO/CNTs, were investigated using a three-point bending test. The flexural strength and flexural modulus for the fiber-reinforced polymer composites are shown in Figure 8a,b, respectively.

As illustrated in Figure 8, the flexural strength and flexural modulus of CFRE without any coating are recorded at 454.78 MPa and 44.04 GPa, respectively. The flexural strength of CCFRE and GCFRE composites was measured at 563.7 and 548.27 MPa, respectively, showing an increase of 23.95% and 20.55% compared to the CFRE composite. Additionally,

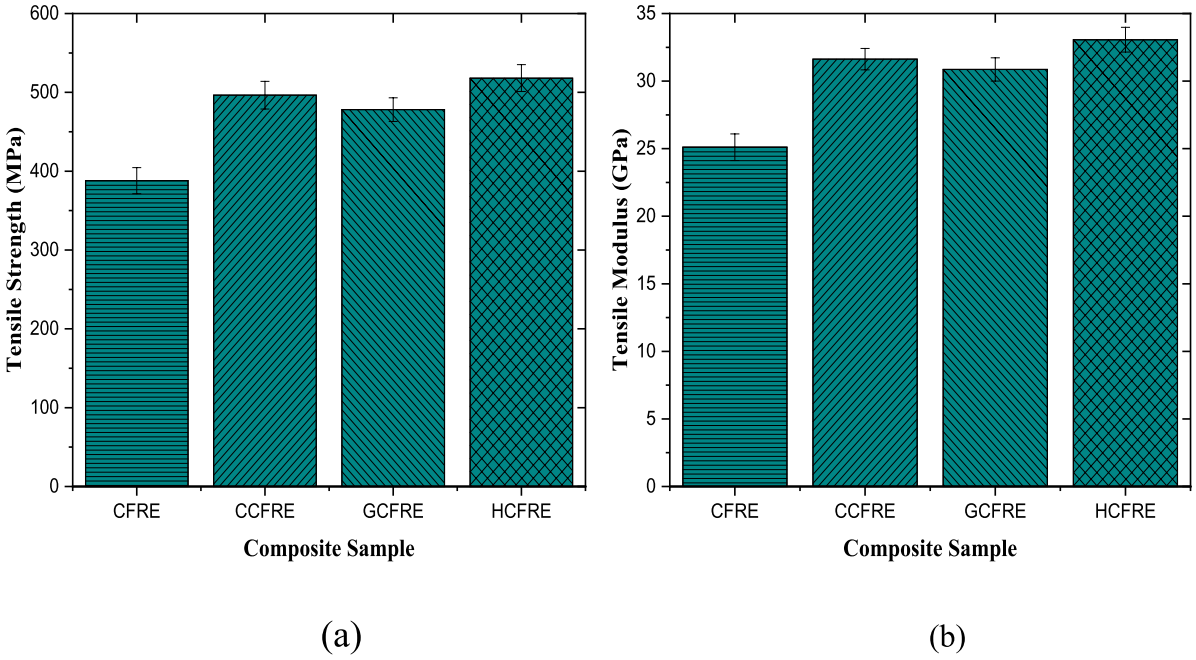


**FIGURE 7** | Tensile strength (a) and tensile modulus (b) of fiber-reinforced polymer composites.

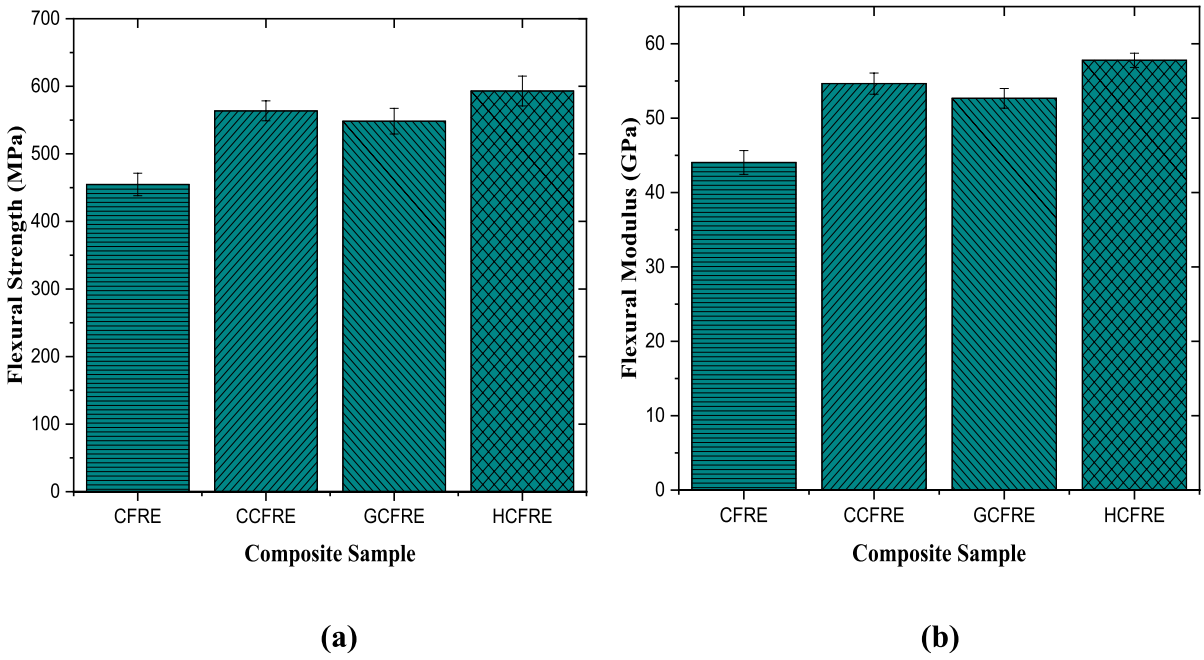


**FIGURE 8** | Flexural strength (a) and flexural modulus (b) of fiber-reinforced polymer composites.

the flexural modulus of CCFRE and GCFRE composites was observed as 54.64 and 52.66 GPa, respectively, demonstrating an increase of 24.06% and 19.57% compared to the CFRE composite. The mechanical properties of the composite were improved by applying a coating consisting of CNTs or GO onto the carbon fiber. This improvement can be attributed to the significant aspect ratio, large surface area, superior stiffness, and flexural modulus of these nanoparticles [47]. From Figure 7, HCFRE demonstrates the highest flexural modulus of 57.77 GPa and flexural strength of 593.07 MPa among all four composite specimens. This represents an increase of 30.40% flexural strength and 31.17% flexural modulus compared to CFRE, demonstrating the synergetic effect of GO and CNTs in the hybrid coating [39].

### 3.7 | Short Beam Shear (SBS) Test

This test is crucial for assessing the ILSS of fiber composites due to their layered structures, which are highly responsive to shear loading. The outcomes of the (SBS) test are depicted in Figure 9, illustrating the effects of coated and uncoated carbon fiber-reinforced epoxy composites. The ILSS value of the CFRE composite is 21.66 MPa. The results indicate that the ILSS of

CCFRE, GCFRE, and HCFRE hybrid-coated CFRP composites is approximately 29.45%, 27.7%, and 38.73% higher, respectively, compared to CFRE composites. The outcome suggests that incorporating GO, CNTs, and a CNTs/GO hybrid into the interphase of fiber-reinforced polymer composites notably enhances their interfacial properties. Among these coatings, the CNTs/GO hybrid coating is the most efficient in enhancing interlaminar shear strength, indicating a clear synergistic effect [39, 48]. The presence of CNTs/GO on the carbon fiber surface enhances the toughness of the epoxy resin near the interface by inducing plastic deformation and extraction of the epoxy resin. This phenomenon aids in improving interfacial stress transfer and strain resistance, thereby allowing for greater energy dissipation during the shear failure process of the interface. Consequently, this effectively enhances the ILSS of fiber-reinforced polymer composites coated with GO/CNTs hybrids [19].

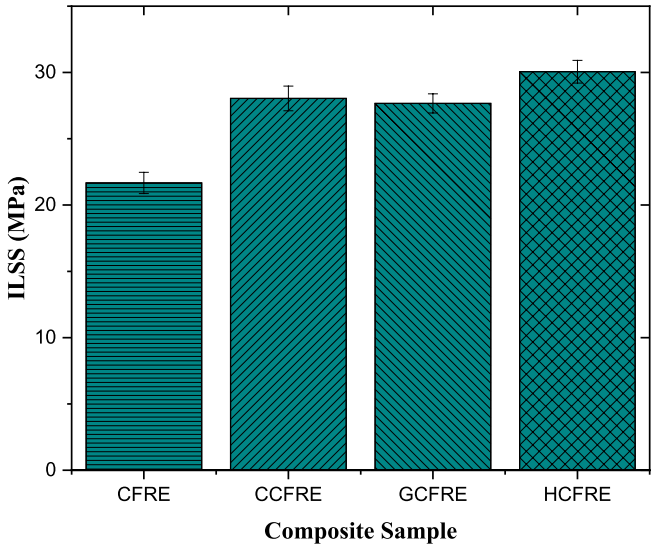


**FIGURE 9** | ILSS of fiber-reinforced epoxy composites.

### 3.8 | Impact Test

The fracture toughness resulting from impact is an important aspect in analyzing the failure of composite materials. When subjected to impacts, composites absorb some energy involved in various failure mechanisms such as interlayer failure, delamination, matrix cracking, and fiber breakage [49]. Figure 10 illustrates the impact energy performance of carbon fiber-reinforced epoxy composites with and without coatings. It is evident that applying coatings of CNTs, GO, and CNTs/GO hybrid nanoparticles onto the carbon fibers enhances the composites' impact strength. The impact energy of the CFRE composite measures 9.13 J/cm$^2$. The findings demonstrate a 26.94% increase in impact energy for CCFRE and a 24.64% increase for GCFRE compared to the CFRE composite. Incorporating CNTs or GO improves the bonding between the filler, matrix, and fiber, enhancing interfacial adhesion [50]. This enhancement contributes to greater impact energy absorption and diminishes interlaminar fracture tendencies within the composites [51]. HCFRE achieves the highest impact energy value of 12.43 J/cm$^2$, marking a 36.36% increment compared to the CFRE composite, owing to the synergistic effects of CNTs/GO. The interlocking mechanism between coated fibers and epoxy significantly enhances the properties of the carbon/epoxy composites [52].

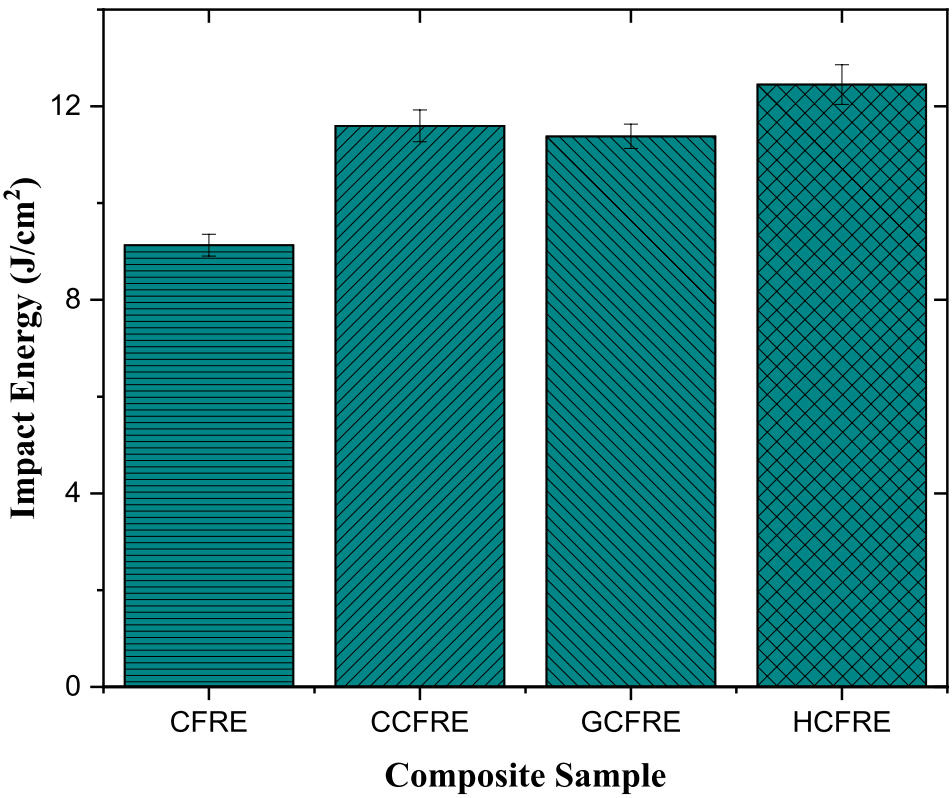


**FIGURE 10** | Impact energy of fiber-reinforced epoxy composites.

### 3.9 | Thermal Conductivity Test

Figure 11 shows the thermal conductivity of the CFRE, CCFRE, GCFRE, and HCFRE composites. Composites containing CNTs (CCFRE) and GO (GCFRE) exhibit thermal conductivities of 0.355 and 0.342 W/mK, respectively, representing a 36.18% and 30.85% increase compared to the CFRE composite. The high specific surface area and superior heat conductivity of GO and CNTs are responsible for this improvement [53, 54]. The HCFRE composite demonstrates the highest thermal conductivity of 0.377 W/mK among the composites due to the synergistic effect of the 1-D rod-like structure of CNTs and the 2-D sheet structure of GO, which creates thermal conductivity bridges, thereby enhancing heat flow [55]. Consequently, introducing CNTs and GO simultaneously into composites significantly improves their thermal conductivity, which in turn improves the tribological performance of the fiber reinforced epoxy composites [43].

### 3.10 | Tribological Testing

#### 3.10.1 | Effect of GO, CNTs, and Hybrid (GO/CNTs) Coating on the Tribological Properties of CFRE Composites

Figure 12 illustrates the evolution of the friction coefficient for CFRE, CCFRE, GCFRE, and HCFRE composites during a 9600-cycle test conducted at room temperature. The test involved a normal load of 40 N, a to and fro sliding frequency of 8 Hz, and a stroke length of 1.5 mm. Initially, composites experienced an increased friction coefficient attributed to matrix plasticization, leading to adhesion between the matrix and the steel ball's surface, along with surface delamination of the composite material [56]. However, carbon fiber fragments emerged after several cycles, acting as third-body particles. These fragments circulated between interacting surfaces, forming a layer of friction that substantially reduced the coefficient of friction before reaching a stable state over a period [31]. It was also observed from Figure 12 that the COF of CCFRE, GCFRE, and HCFRE was lower than that of the CFRE composite because of the self-lubricating properties, high load-bearing capacity, and high wear resistance of GO and CNTs [57].

Figure 13 provides clear evidence that the CCFRE, GCFRE, and HCFRE composites experience reduced weight loss and specific wear rates compared to the CFRE composite. This difference can be ascribed to incorporating CNTs, GO, or both, which were applied as a coating on the carbon fiber within the polymer composite. The composite's resistance to wear was eventually improved by this coating's improvement of interfacial adhesion. The CFRE composite has a specific wear rate of 23.62($*10^{-4}$ $mm^3$/Nm). The study found a 27.26% decrease in specific wear rate for CCFRE compared to CFRE, suggesting that CNTs at the fiber-matrix interface promote the formation of a durable tribo-film, reducing wear [58]. Additionally, CNTs act as micro-bearings, converting sliding friction to rolling friction, further reducing wear and COF [59, 60]. Similarly, GCFRE showed a significant 23.45% decrease in specific wear rate compared to CFRE, attributed to solid film formation by GO due to weak van der Waals forces between GO sheets [61]. The improved mechanical interlocking induced from the wrinkled rough surface of GO enhances interfacial adhesion between the matrix and fiber, indicating that adding GO to carbon fiber/Epoxy composites improves wear resistance by reducing abrasive wear [62, 63]. HCFRE observed the minimum specific wear rate, which was 42.84% less than the CFRE composite because of the synergetic effect of CNTs/GO hybrid-coated carbon fiber reinforced polymer composite. Flexible carbon nanotubes (CNTs) can penetrate between GO, preventing them from aggregating face-to-face. Van der Waals forces cause GO to infiltrate between CNTs and create complementary structures that interact to prevent restacking [64]. This suggests that the hybrid coating of GO and CNTs can easily form a 3D structure of hybrid carbon nanomaterials, leading to increased surface area. This enhanced surface area improves contact and interlocking at the interface between the matrix and carbon fibers, ultimately enhancing interfacial adhesion. Moreover, incorporating GO

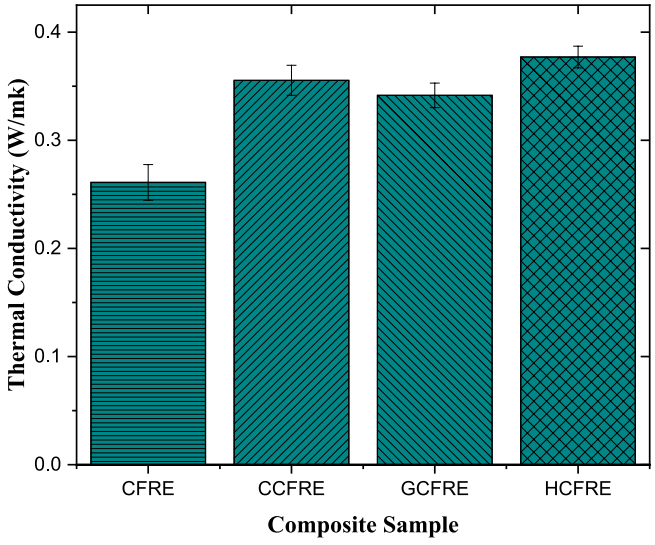


**FIGURE 11** | Thermal conductivity of fiber-reinforced epoxy composites.

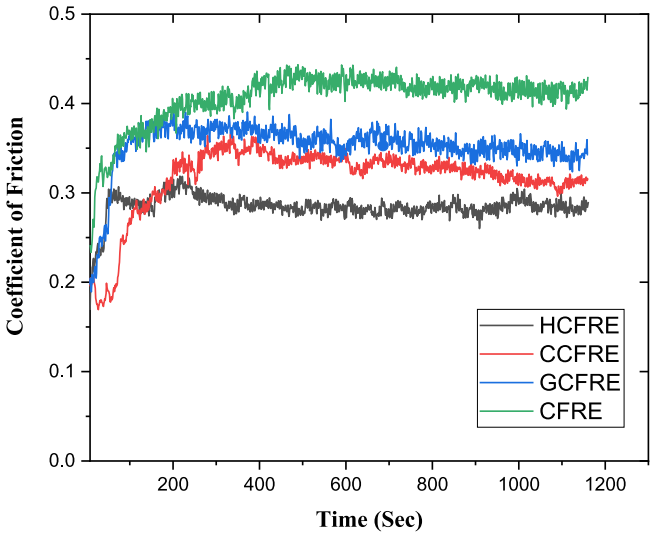


**FIGURE 12** | Coefficient of friction versus time for CFRE, CCFRE, GCFRE, and composite at (40 N, 8 Hz).

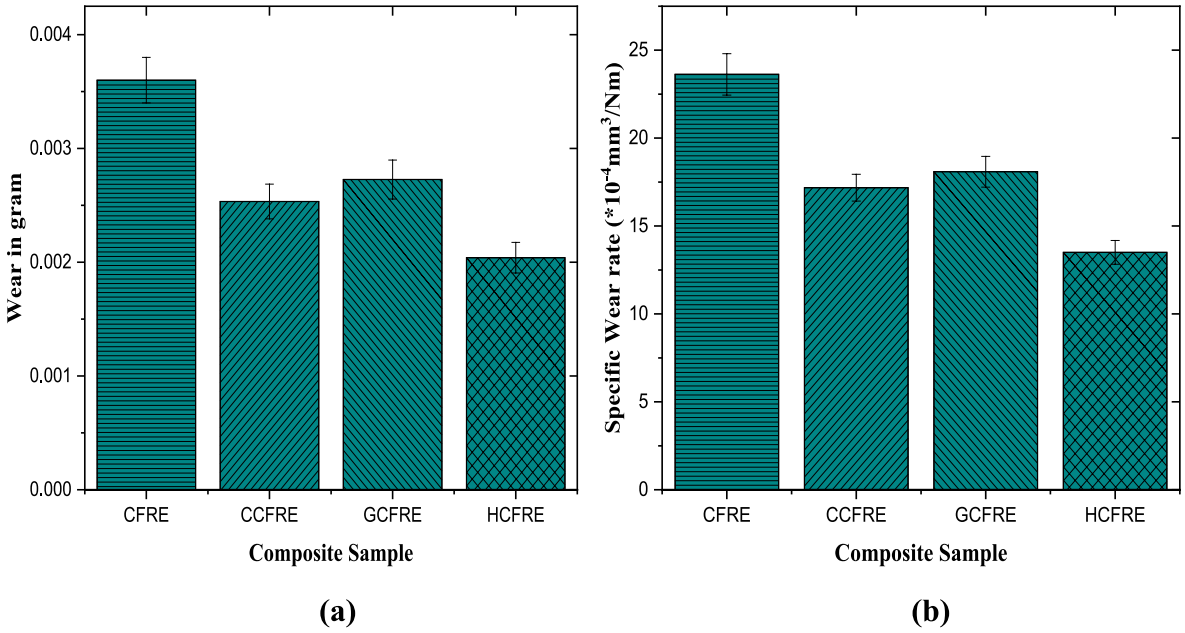


**FIGURE 13** | Variation of (a) wear in gram and (b) specific wear rate of CFRE, CCFRE, GCFRE, and HCFRE composite at (40 N, 8 Hz).

and CNTs will enhance wear resistance by uniformly dispersing stress throughout the matrix [65]. The findings showed great enhancement in friction and wear properties due to the surface modification of carbon fiber with CNTs and GO [66].

### 3.10.2 | Effect of Load on Friction Coefficient of Fiber-Reinforced Polymer Composite

The COF values for CFRE, CCFRE, GCFRE, and HCFRE composites are shown in Figure 14 with varied normal loads (30, 40, 50, and 60 N) at a constant frequency of 8 Hz. The findings suggest that as the applied normal load rises, the coefficient of friction (COF) also increases across different polymer composite samples. This phenomenon can be attributed to the increased contact pressure between the steel ball and the specimen under higher loads, potentially elevating the interface temperature and reinforcing the adhesive component of friction [67]. Furthermore, asperities penetrate significantly at higher loads, increasing the frictional force and contributing significantly to the abrasion component of the friction coefficient [30]; thus, the increase in the COF at higher normal loads can likely be attributed to these factors. At a normal load of 30 N, the HCFRE composite demonstrates the lowest COF value of 0.234, while the CFRE composite exhibits the highest COF value of 0.41 at a normal load of 60 N.

### 3.10.3 | Effect of Sliding Frequency on Friction Coefficient of Fiber-Reinforced Polymer Composite

The COF values for CFRE, CCFRE, GCFRE, and HCFRE polymer composites are shown in Figure 15 at different frequencies (6, 8, 10, and 12 Hz) under a constant normal load of 40 N. For all four polymer composites, the findings show a drop in COF with increased sliding frequency. This decline is explained by the higher reciprocating sliding frequency, which causes the

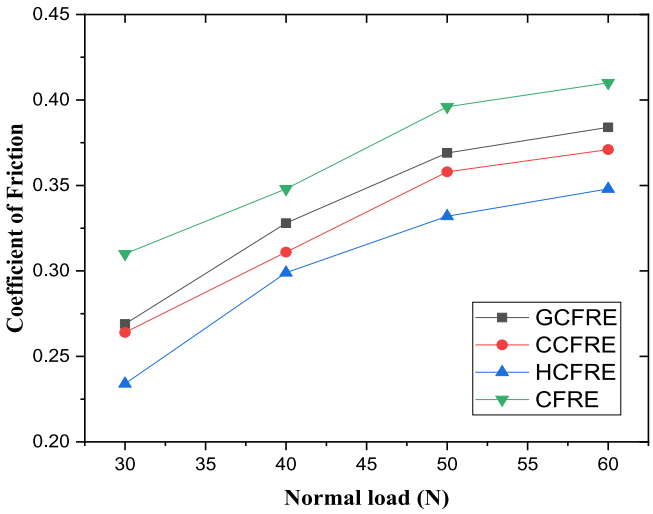


**FIGURE 14** | Variation of friction coefficient with load at a constant frequency of 8 Hz.

polymer matrix to soften and undergo plastic deformation [68]. By lowering adhesion force and plowing action, carbon fibers improve the polymer composite's frictional properties. A similar tendency of COF decreasing with sliding frequency was also observed by Guo et al. [69] who attributed this to surface softening brought on by frictional heating. With a friction coefficient value of 0.277 at 12 Hz, the HCFRE composite had the lowest value, while at 6 Hz, the CFRE composite had the highest value, 0.354.

## 3.11 | SEM Analysis of Fracture Surface

The variations in interfacial performance trends observed among CFRE, CCFRE, GCFRE, and HCFRE composites reinforced with CNTs and GO are primarily attributed to the formation of distinct interphases between the carbon fibers and

the resin matrix. This hypothesis is substantiated by the SEM micrographs presented in Figure 16. As shown in Figure 16a, the CFRE composite exhibits a debonded fiber surface with minimal residual epoxy, indicating weak interfacial adhesion and identifying fiber–matrix debonding as the dominant failure mechanism [70]. In contrast, the incorporation of nanoparticles in CCFRE, GCFRE, and HCFRE composites significantly enhanced matrix adhesion to the fiber surfaces, as evident from the increased matrix residues observed in Figure 16b–d. This improvement suggests strengthened interfacial interactions resulting from the presence of CNTs and GO. Notably, the HCFRE composite displayed the highest degree of matrix retention on the fiber surface, along with a marked reduction in interfacial defects such as cracks and voids. Correspondingly, the dominant failure mechanism shifted from fiber–matrix debonding to matrix deformation and fracture, indicating a substantial enhancement in interfacial bonding strength and overall adhesion in the nanoparticle-coated fiber-reinforced composite [66].

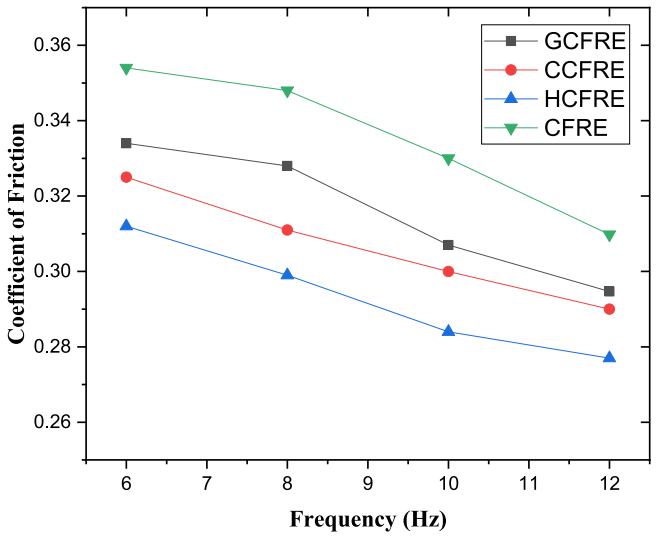


**FIGURE 15** | Variation of friction coefficient with frequency at a constant load of 40 N.

### 3.12 | SEM Analysis of Worn Surface

Figure 17 displays the SEM pictures of the worn surfaces of the CFRE, CCFRE, GCFRE, and HCFRE polymer composites under the identical conditions (40 N, 8 Hz). Figure 17a shows that maximum breakage of the matrix and fiber was found in the CFRE composite because of the poor interfacial adhesion and mechanical interlocking between the fibers and matrix [71]. In the CFRE composites, the surface displayed extensive matrix breakdown, with most fibers in the top layer disconnected. The worn surfaces from sliding exhibited notable fiber breakage, debonding, and removal, along with instances of fiber pull-out due to inadequate fiber-matrix adhesion. In CNTs, GO, and hybrid coated fiber

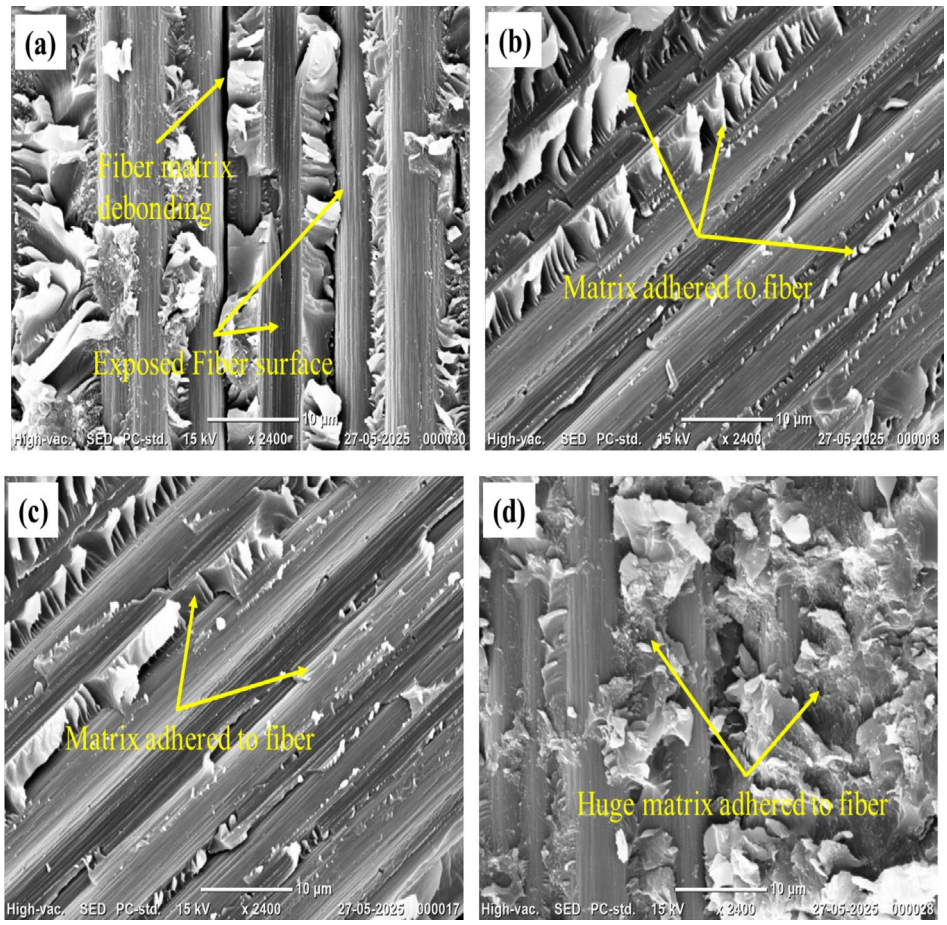


**FIGURE 16** | SEM images of fractured surfaces of (a) CFRE, (b) CCFRE, (c) GCFRE, and (d) HCFRE.

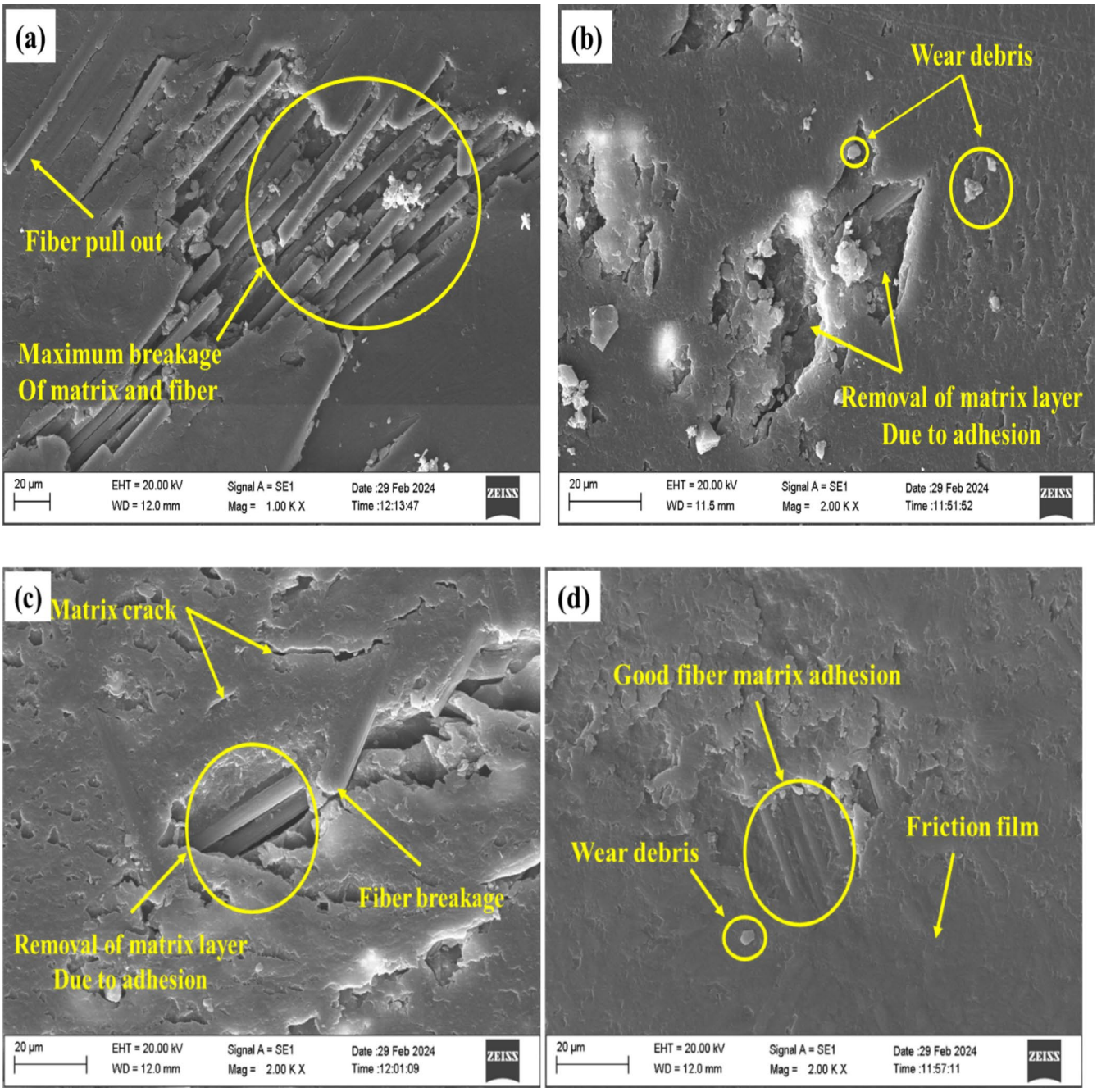


**FIGURE 17** | SEM images of worn surfaces of (a) CFRE, (b) CCFRE, (c) GCFRE, and (d) HCFRE under the same condition (40 N, 8 Hz).

polymer composite samples, as shown in Figure 17b–d, minimal empty fiber slots, fiber damage, and matrix removal due to adhesion were observed, indicating enhanced bond strength between fibers and the matrix, thus hindering fiber pull-out [1].

Additionally, residual stresses generated during curing can lead to stress concentration and separation between the fiber and matrix. Nanoparticles coated on fiber alleviate these stresses through mechanical locking, enhancing interfacial strength between fiber and matrix, increasing the stress required for fiber breakage and pull-out [72]. From Figure 17d, it was clear that the HCFRE composite exhibited excellent fiber-matrix adhesion and minimal removal of the matrix layer, attributed to the combined effect of CNTs and GO. This synergy likely arises from the high thermal conductivity of the composite, which aids in dissipating frictional heat from the interface region, along with the lubricating effect of CNTs and GO [73]. Additionally, in the HCFRE composite, wear debris containing CNTs and GO adhered to the counter face, forming a friction film layer at the interface. This layer significantly reduced the coefficient of friction and specific wear rate.

## 4 | Conclusions

This article investigates the application of CNTs, GO, and their hybrid (CNTs/GO) coatings on carbon fibers to enhance interfacial properties and mechanical bonding in epoxy composites. The nanoparticle-coated carbon fibers result in heightened surface roughness, facilitating better adherence with the matrix

material and consequently improving mechanical integration. TGA showcases improved thermal stability for the modified composites attributed to the protective barriers provided by GO and CNTs. Integrating 2D GO and 1D CNTs resulted in a three-dimensional network structure, exhibiting a significant synergistic effect in enhancing the mechanical properties and interfacial of fiber-reinforced polymer composites. Compared to CFRP composites with individual CNTs or GO coatings deposited on carbon fiber surfaces, those with the CNTs/GO hybrid coating showed the highest interlaminar shear strength (ILSS), flexural strength, tensile strength, and hardness, with enhancements of 38.73%, 30.40%, 33.53%, and 32.64%, respectively, compared to CFRE composites. The fracture toughness, tensile, and flexural modulus were also maximum for the HCFRE composite, with improvements of 36.36%, 31.66%, and 57.68%, respectively, over the CFRE composite. Furthermore, the CNTs/GO hybrid coating improves adherence to the matrix, resulting in a 42.84% reduction in the specific wear rate. The COF decreases with the increase in sliding frequency; however, it increases with the increase in load. The HCFRE composite demonstrates the highest thermal conductivity of 0.377 W/mK among the four composites. SEM analysis depicts enhanced fiber-matrix adhesion and minimal surface damage in the modified composites, highlighting the efficacy of the coatings in improving interfacial bonding. Overall, the HCFRE composite exhibits maximum enhancements in mechanical, thermal, and tribological properties, making it a promising material for various engineering applications requiring high-performance materials with improved durability and reliability.


### Acknowledgments

The financial support provided by the SERB through the SRG grant (SRG/2020/001811) and DRDO (DFTM/10/3855/M/12/PM-10/003/D (R&D)) is gratefully acknowledged.


### Conflicts of Interest

The authors declare no conflicts of interest.

### Data Availability Statement

The data that support the findings of this study are available from the corresponding author upon reasonable request.

### References


1. S. Kumar, K. K. Singh, and J. Ramkumar, "Comparative Study of the Influence of Graphene Nanoplatelets Filler on the Mechanical and Tribological Behavior of Glass Fabric-Reinforced Epoxy Composites," *Polymer Composites* 41, no. 12 (2020): 5403–5417.

2. R. Luo, X. Huai, J. Qu, H. Ding, and S. Xu, "Effect of Heat Treatment on the Tribological Behavior of 2D Carbon/Carbon Composites," *Carbon* 41, no. 14 (2003): 2693–2701.

3. F.-H. Su, Z. Z. Zhang, K. Wang, W. Jiang, X. H. Men, and W. M. Liu, "Friction and Wear Properties of Carbon Fabric Composites Filled With Nano-$Al_2O_3$ and Nano-Si3N4," *Composites Part A: Applied Science and Manufacturing* 37, no. 9 (2006): 1351–1357.

4. Z.-z. Zhang, H.-j. Zhang, F. Guo, K. Wang, and W. Jiang, "Enhanced Wear Resistance of Hybrid PTFE/Kevlar Fabric/Phenolic Composite by Cryogenic Treatment," *Journal of Materials Science* 44 (2009): 6199–6205.

5. M. Singh, R. Yadav, R. Kumar, S. Dodla, and R. K. Gautam, "Development and Characterization of Hybrid Polymer Composite Materials With Reinforcement of Glass/Carbon Fibers for Enhanced Mechanical Properties: An Experimental and Numerical Approach," *Journal of the Textile Institute* 116 (2024): 1–1543.

6. R. Rattan, J. Bijwe, and M. Fahim, "Optimization of Weave of Carbon Fabric for Best Combination of Strength and Tribo-Performance of Polyetherimide Composites in Adhesive Wear Mode," *Wear* 264, no. 1–2 (2008): 96–105.

7. L.-H. Sun, Z.-G. Yang, and X.-H. Li, "Tensile and Tribological Properties of PTFE and Nanoparticles Modified Epoxy-Based Polyester Fabric Composites," *Materials Science and Engineering A* 497, no. 1–2 (2008): 487–494.

8. J. Bijwe and R. Rattan, "Influence of Weave of Carbon Fabric in Polyetherimide Composites in Various Wear Situations," *Wear* 263, no. 7–12 (2007): 984–991.

9. K. K. Chawla and K. K. Chawla, "Carbon Fiber Composites," in *Composite Materials: Science and Engineering* (Springer Science & Business Media, 1987), 252–277.

10. Q. An, A. N. Rider, and E. T. Thostenson, "Hierarchical Composite Structures Prepared by Electrophoretic Deposition of Carbon Nanotubes Onto Glass Fibers," *ACS Applied Materials and Interfaces* 5, no. 6 (2013): 2022–2032.

11. B. Vieille, M. Chabchoub, and C. Gautrelet, "Influence of Matrix Ductility and Toughness on Strain Energy Release Rate and Failure Behavior of Woven-Ply Reinforced Thermoplastic Structures at High Temperature," *Composites Part B: Engineering* 132 (2018): 125–140.

12. A. Godara, L. Gorbatikh, G. Kalinka, et al., "Interfacial Shear Strength of a Glass Fiber/Epoxy Bonding in Composites Modified With Carbon Nanotubes," *Composites Science and Technology* 70, no. 9 (2010): 1346–1352.

13. H. Cen, Y. Kang, Z. Lei, Q. Qin, and W. Qiu, "Micromechanics Analysis of Kevlar-29 Aramid Fiber and Epoxy Resin Microdroplet Composite by Micro-Raman Spectroscopy," *Composite Structures* 75, no. 1–4 (2006): 532–538.

14. M. Sharma, S. Gao, E. Mäder, H. Sharma, L. Y. Wei, and J. Bijwe, "Carbon Fiber Surfaces and Composite Interphases," *Composites Science and Technology* 102 (2014): 35–50.

15. K. T. Nguyen, K. T. Q. Nguyen, S. Navaratnam, et al., "Fire Safety of Composites in Prefabricated Buildings: From Fibre Reinforced Polymer to Textile Reinforced Concrete," *Composites Part B, Engineering* 187 (2020): 107815.

16. B. Ravichandran and M. Balasubramanian, "Joining Methods for Fiber Reinforced Polymer (FRP) Composites—A Critical Review," *Composites Part A, Applied Science and Manufacturing* 186 (2024): 108394.

17. R. Malekimoghadam and U. Icardi, "Prediction of Mechanical Properties of Carbon Nanotube–Carbon Fiber Reinforced Hybrid Composites Using Multi-Scale Finite Element Modelling," *Composites Part B: Engineering* 177 (2019): 107405.

18. W. Qin, F. Vautard, L. T. Drzal, and J. Yu, "Modifying the Carbon Fiber–Epoxy Matrix Interphase With Graphite Nanoplatelets," *Polymer Composites* 37, no. 5 (2016): 1549–1556.

19. C. Xiao, Y. Tan, X. Wang, L. Gao, L. Wang, and Z. Qi, "Study on Interfacial and Mechanical Improvement of Carbon Fiber/Epoxy Composites by Depositing Multi-Walled Carbon Nanotubes on Fibers," *Chemical Physics Letters* 703 (2018): 8–16.

20. Y. J. Kwon, Y. Kim, H. Jeon, S. Cho, W. Lee, and J. U. Lee, "Graphene/Carbon Nanotube Hybrid as a Multi-Functional Interfacial Reinforcement for Carbon Fiber-Reinforced Composites," *Composites Part B: Engineering* 122 (2017): 23–30.

21. K. Ismail, K. I. Ismail, M. T. H. Sultan, A. U. M. Shah, M. Jawaid, and S. N. A. Safri, "Low Velocity Impact and Compression After Impact

Properties of Hybrid Bio-Composites Modified With Multi-Walled Carbon Nanotubes," *Composites Part B, Engineering* 163 (2019): 455–463.

22. M. Singh, S. Dodla, R. K. Gautam, and V. Chauhan, "Enhancement of Mechanical and Tribological Properties in Glass Fiber-Reinforced Polymer Composites With Multi-Walled Carbon Nanotubes and ANN-Based COF Prediction," *Composite Interfaces* 32 (2024): 1–21.

23. X. Liang and Q. Cheng, "Synergistic Reinforcing Effect From Graphene and Carbon Nanotubes," *Composites Communications* 10 (2018): 122–128.

24. M. Li, Y. Gu, Y. Liu, Y. Li, and Z. Zhang, "Interfacial Improvement of Carbon Fiber/Epoxy Composites Using a Simple Process for Depositing Commercially Functionalized Carbon Nanotubes on the Fibers," *Carbon* 52 (2013): 109–121.

25. X. Zhou, X. Zhang, S. Xu, S. Wu, Q. Liu, and Z. Fan, "Evaluation of Thermo-Mechanical Properties of Graphene/Carbon-Nanotubes Modified Asphalt With Molecular Simulation," *Molecular Simulation* 43, no. 4 (2017): 312–319.

26. X. Zhang, X. Fan, C. Yan, et al., "Interfacial Microstructure and Properties of Carbon Fiber Composites Modified With Graphene Oxide," *ACS Applied Materials and Interfaces* 4, no. 3 (2012): 1543–1552.

27. W. Qin, F. Vautard, L. T. Drzal, and J. Yu, "Mechanical and Electrical Properties of Carbon Fiber Composites With Incorporation of Graphene Nanoplatelets at the Fiber–Matrix Interphase," *Composites Part B: Engineering* 69 (2015): 335–341.

28. J. Naveen, M. Jawaid, E. S. Zainudin, M. Thariq Hameed Sultan, and R. Yahaya, "Improved Mechanical and Moisture-Resistant Properties of Woven Hybrid Epoxy Composites by Graphene Nanoplatelets (GNP)," *Materials* 12, no. 8 (2019): 1249.

29. R. Yadav, M. Singh, D. Shekhawat, S. Y. Lee, and S. J. Park, "The Role of Fillers to Enhance the Mechanical, Thermal, and Wear Characteristics of Polymer Composite Materials: A Review," *Composites Part A: Applied Science and Manufacturing* 175 (2023): 107775.

30. M. Singh, S. Dodla, R. K. Gautam, and V. K. Srivastava, "Effect of Load, Sliding Frequency, and Temperature on Tribological Properties of Graphene Nanoplatelets Coated Carbon Fiber Reinforced Polymer Composites," *Journal of Composite Materials* 57, no. 1 (2023): 121–132.

31. M. Singh, S. Dodla, and R. Gautam, "Mechanical and Tribological Properties of CNTs Coated Aramid Fiber-Reinforced Epoxy Composites," *Composites Part A, Applied Science and Manufacturing* 179 (2024): 108061.

32. S. Behera, R. K. Gautam, and S. Mohan, "The Effect of Eco-Friendly Chemical Treatment on Sisal Fiber and Its Epoxy Composites: Thermal, Mechanical, Tribological and Morphological Properties," *Cellulose* 29, no. 17 (2022): 9055–9072.

33. S. Sabagh, A. A. Azar, and A. R. Bahramian, "High Temperature Ablation and Thermo-Physical Properties Improvement of Carbon Fiber Reinforced Composite Using Graphene Oxide Nanopowder," *Composites Part A, Applied Science and Manufacturing* 101 (2017): 326–333.

34. Z. Eslami, F. Yazdani, and M. A. Mirzapour, "Thermal and Mechanical Properties of Phenolic-Based Composites Reinforced by Carbon Fibres and Multiwall Carbon Nanotubes," *Composites Part A: Applied Science and Manufacturing* 72 (2015): 22–31.

35. P. Jojibabu, G. D. J. Ram, A. P. Deshpande, and S. R. Bakshi, "Effect of Carbon Nano-Filler Addition on the Degradation of Epoxy Adhesive Joints Subjected to Hygrothermal Aging," *Polymer Degradation and Stability* 140 (2017): 84–94.

36. J. Cui, Y. Yan, J. Liu, and Q. Wu, "Phenolic Resin-MWNT Nanocomposites Prepared Through an In Situ Polymerization Method," *Polymer Journal* 40, no. 11 (2008): 1067–1073.

37. J.-M. Park, D. J. Kwon, Z. J. Wang, et al., "Effects of Carbon Nanotubes and Carbon Fiber Reinforcements on Thermal Conductivity and Ablation Properties of Carbon/Phenolic Composites," *Composites Part B: Engineering* 67 (2014): 22–29.

38. C. Hu, X. Liao, Q. H. Qin, and G. Wang, "The Fabrication and Characterization of High Density Polyethylene Composites Reinforced by Carbon Nanotube Coated Carbon Fibers," *Composites Part A: Applied Science and Manufacturing* 121 (2019): 149–156.

39. W. Qin, C. Chen, J. Zhou, and J. Meng, "Synergistic Effects of Graphene/Carbon Nanotubes Hybrid Coating on the Interfacial and Mechanical Properties of Fiber Composites," *Materials* 13, no. 6 (2020): 1457.

40. B. Kamesh, L. K. Singh, M. K. Kassa, and A. B. Arumugam, "Synergetic Effect of Incorporating Graphene, CNT and Hybrid Nanoparticles on the Mechanical Properties of Glass Fiber Reinforced Epoxy Laminated Composites," *Cogent Engineering* 10, no. 1 (2023): 2232604.

41. M. R. Zakaria, M. H. Abdul Kudus, H. Md Akil, et al., "Comparative Study of Single-Layer Graphene and Single-Walled Carbon Nanotube-Filled Epoxy Nanocomposites Based on Mechanical and Thermal Properties," *Polymer Composites* 40, no. S2 (2019): E1840–E1849.

42. K. J. Kim, J. Kim, W. R. Yu, J. H. Youk, and J. Lee, "Improved Tensile Strength of Carbon Fibers Undergoing Catalytic Growth of Carbon Nanotubes on Their Surface," *Carbon* 54 (2013): 258–267.

43. B. Wang, Q. Fu, Y. Liu, T. Yin, and Y. Fu, "The Synergy Effect in Tribological Performance of Paper-Based Composites by MWCNT and GNPs," *Tribology International* 123 (2018): 200–208.

44. J. Llorente, B. Román-Manso, P. Miranzo, and M. Belmonte, "Tribological Performance Under Dry Sliding Conditions of Graphene/Silicon Carbide Composites," *Journal of the European Ceramic Society* 36, no. 3 (2016): 429–435.

45. M. R. Zakaria, H. M. Akil, M. H. A. Kudus, and S. S. M. Saleh, "Enhancement of Tensile and Thermal Properties of Epoxy Nanocomposites Through Chemical Hybridization of Carbon Nanotubes and Alumina," *Composites Part A: Applied Science and Manufacturing* 66 (2014): 109–116.

46. I. Taraghi, A. Fereidoon, and A. Mohyeddin, "The Effect of MWCNTs on the Mechanical Properties of Woven Kevlar/Epoxy Composites," *Steel and Composite Structures* 17, no. 6 (2014): 825–834.

47. F. Azimpour-Shishevan, H. Akbulut, and M. Mohtadi-Bonab, "Synergetic Effects of Carbon Nanotube and Graphene Addition on Thermo-Mechanical Properties and Vibrational Behavior of Twill Carbon Fiber Reinforced Polymer Composites," *Polymer Testing* 90 (2020): 106745.

48. X. Yao, J. Jiang, C. Xu, L. Zhou, C. Deng, and J. Wang, "Improved Interfacial Properties of Carbon Fiber/Epoxy Composites Through Graphene Oxide-Assisted Deposition of Carbon Nanotubes on Carbon Fiber Surface," *Fibers and Polymers* 18 (2017): 1323–1329.

49. B. Park, S. C. Kim, and B. Jung, "Interlaminar Fracture Toughness of Carbon Fiber/Epoxy Composites Using Short Kevlar Fiber and/or Nylon-6 Powder Reinforcement," *Polymers for Advanced Technologies* 8, no. 6 (1997): 371–377.

50. A. Namdev, A. Telang, and R. Purohit, "Synthesis and Mechanical Characterization of Epoxy Hybrid Composites Containing Graphene Nanoplatelets," *Proceedings of the Institution of Mechanical Engineers, Part C: Journal of Mechanical Engineering Science* 236, no. 14 (2022): 7984–7998.

51. N. C. Adak, S. Chhetri, T. Kuila, N. C. Murmu, P. Samanta, and J. H. Lee, "Effects of Hydrazine Reduced Graphene Oxide on the Inter-Laminar Fracture Toughness of Woven Carbon Fiber/Epoxy Composite," *Composites Part B: Engineering* 149 (2018): 22–30.

52. A. Sarwar, Z. Mahboob, R. Zdero, and H. Bougherara, "Mechanical Characterization of a New Kevlar/Flax/Epoxy Hybrid Composite in a Sandwich Structure," *Polymer Testing* 90 (2020): 106680.

53. Z. Gao and L. Zhao, "Effect of Nano-Fillers on the Thermal Conductivity of Epoxy Composites With Micro-Al2O3 Particles," *Materials and Design (1980–2015)* 66 (2015): 176–182.

54. B. Li, S. Dong, X. Wu, C. Wang, X. Wang, and J. Fang, "Anisotropic Thermal Property of Magnetically Oriented Carbon Nanotube/Graphene Polymer Composites," *Composites Science and Technology* 147 (2017): 52–61.

55. S. Song and Y. Zhang, "Carbon Nanotube/Reduced Graphene Oxide Hybrid for Simultaneously Enhancing the Thermal Conductivity and Mechanical Properties of Styrene-Butadiene Rubber," *Carbon* 123 (2017): 158–167.

56. V. Srivastava, V. K. Srivastava, P. Kumar, T. Quadflieg, and C. Greb, "Friction and Wear Behavior of GNPs Functionalized Carbon Fiber Reinforced Polymer Matrix Composites Under High-Frequency Reciprocating Conditions," *Materials Research Express* 6, no. 12 (2020): 125357.

57. B. Chen, X. Li, Y. Jia, et al., "Fabrication of Ternary Hybrid of Carbon Nanotubes/Graphene Oxide/$MoS_2$ and Its Enhancement on the Tribological Properties of Epoxy Composite Coatings," *Composites Part A: Applied Science and Manufacturing* 115 (2018): 157–165.

58. Z. Lin, J. Yang, X. Jia, Y. Li, and H. Song, "Polydopamine/FeOOH-Modified Interface in Carbon Cloth/Polyimide Composites for Improved Mechanical/Tribological Properties," *Materials Chemistry and Physics* 243 (2020): 122677.

59. C. Min, D. Liu, C. Shen, et al., "Unique Synergistic Effects of Graphene Oxide and Carbon Nanotube Hybrids on the Tribological Properties of Polyimide Nanocomposites," *Tribology International* 117 (2018): 217–224.

60. M. R. Zakaria, M. H. Abdul Kudus, H. Md. Akil, and M. Z. Mohd Thirmizir, "Comparative Study of Graphene Nanoparticle and Multiwall Carbon Nanotube Filled Epoxy Nanocomposites Based on Mechanical, Thermal and Dielectric Properties," *Composites Part B: Engineering* 119 (2017): 57–66.

61. N. Sharma, S. Kumar, and K. Singh, "Taguchi's DOE and Artificial Neural Network Analysis for the Prediction of Tribological Performance of Graphene Nano-Platelets Filled Glass Fiber Reinforced Epoxy Composites Under the Dry Sliding Condition," *Tribology International* 172 (2022): 107580.

62. X.-J. Shen, X. Q. Pei, Y. Liu, and S. Y. Fu, "Tribological Performance of Carbon Nanotube–Graphene Oxide Hybrid/Epoxy Composites," *Composites Part B: Engineering* 57 (2014): 120–125.

63. A. Namdev, A. Telang, and R. Purohit, "Experimental Investigation on Mechanical and Wear Properties of GNP/Carbon Fiber/Epoxy Hybrid Composites," *Materials Research Express* 9, no. 2 (2022): 025303.

64. L. Yue, G. Pircheraghi, S. A. Monemian, and I. Manas-Zloczower, "Epoxy Composites With Carbon Nanotubes and Graphene Nanoplatelets–Dispersion and Synergy Effects," *Carbon* 78 (2014): 268–278.

65. S. H. Yetgin, "Impact of Multi-Walled Carbon Nanotube and Graphene Oxide on Abrasive Wear Performance of Polypropylene," *Research on Engineering Structures and Materials* 7 (2021): 157–171.

66. M. Lai, L. Jiang, X. Wang, H. Zhou, Z. Huang, and H. Zhou, "Effects of Multi-Walled Carbon Nanotube/Graphene Oxide-Based Sizing on Interfacial and Tribological Properties of Continuous Carbon Fiber/Poly (Ether Ether Ketone) Composites," *Materials Chemistry and Physics* 276 (2022): 125344.

67. S. Behera, R. K. Gautam, S. Mohan, and A. Chattopadhyay, "Hemp Fiber Surface Modification: Its Effect on Mechanical and Tribological Properties of Hemp Fiber Reinforced Epoxy Composites," *Polymer Composites* 42, no. 10 (2021): 5223–5236.

68. Y. Chen, J. Zhang, L. Wang, et al., "Tribological Behavior of Carbon-Fiber-Reinforced Polymer With Highly Oriented Graphite Nanoplatelets," *Tribology International* 186 (2023): 108577.

69. F. Guo, Z. Z. Zhang, W. M. Liu, F. H. Su, and H. J. Zhang, "Influence of Solid Lubricant Reinforcement on Wear Behavior of Kevlar Fabric Composites," *Journal of Applied Polymer Science* 110, no. 3 (2008): 1771–1777.

70. A. Vedrtnam and S. P. Sharma, "Study on the Performance of Different Nano-Species Used for Surface Modification of Carbon Fiber for Interface Strengthening," *Composites Part A: Applied Science and Manufacturing* 125 (2019): 105509.

71. M. Sharma, J. Bijwe, E. Mäder, and K. Kunze, "Strengthening of CF/PEEK Interface to Improve the Tribological Performance in Low Amplitude Oscillating Wear Mode," *Wear* 301, no. 1–2 (2013): 735–739.

72. E. F. Sukur and G. Onal, "Graphene Nanoplatelet Modified Basalt/Epoxy Multi-Scale Composites With Improved Tribological Performance," *Wear* 460 (2020): 203481.

73. J. N. Panda, J. Bijwe, and R. K. Pandey, "Variation in Size of Graphite Particles and Its Cascading Effect on the Performance Properties of PAEK Composites," *Composites Part B: Engineering* 182 (2020): 107641.